Uncovering and Circumventing Noise in Quantum Algorithms via Metastability

Antonio Sannia, ^{1, 2, 3, *} Pratik Sathe, ^{1, 4} and Luis Pedro García-Pintos¹

¹ Quantum and Condensed Matter Physics Group (T-4), Theoretical Division,

Los Alamos National Laboratory, Los Alamos, New Mexico 87545, USA

² Institute for Cross-Disciplinary Physics and Complex Systems (IFISC) UIB-CSIC,

Campus Universitat Illes Balears, 07122, Palma de Mallorca, Spain

³ USRA Research Institute for Advanced Computer Science (RIACS), USA

⁴ Information Science & Technology Institute, Los Alamos National Laboratory, Los Alamos, NM 87545, USA

The presence of noise is the primary challenge in realizing fault-tolerant quantum computers. In this work, we introduce and experimentally validate a novel strategy to circumvent noise by exploiting the phenomenon of metastability, where a dynamical system exhibits long-lived intermediate states. We demonstrate that if quantum hardware noise exhibits metastability, both digital and analog algorithms can be designed in a noise-aware fashion to achieve intrinsic resilience. We develop a general theoretical framework and introduce an efficiently computable noise resilience metric that avoids the need for full classical simulation of the quantum algorithm. We illustrate the use of our framework with applications to variational quantum algorithms and analog adiabatic state preparation. Crucially, we provide experimental evidence supporting the presence of metastable noise in gate-model quantum processors as well as quantum annealing devices. Thus, we establish that the intrinsic nature of noise in near-term quantum hardware can be leveraged to inform practical implementation strategies, enabling the preparation of final noisy states that more closely approximate the ideal ones.

I. INTRODUCTION

Noise and decoherence remain the primary obstacles for experimentally demonstrating quantum advantages over classical methods [1, 2]. Despite significant advances in hardware design, current error rates remain too high to enable large-scale fault-tolerant computation. Consequently, developing strategies to mitigate or even exploit noise has become a central goal in quantum information science [3]. In this work, we introduce a novel approach to characterizing and alleviating the effects of noise in quantum algorithms. Our key insight is that noise can exhibit a structured behavior that can be harnessed to protect quantum computations. In particular, we focus on metastability [4], a phenomenon in which a dynamical system exhibits long-lived intermediate states before eventual relaxation.

Metastable states have been extensively studied in classical contexts, including statistical physics [5], chemical systems [6], and neuroscience [7]. Interestingly, metastability also arises in quantum systems [8] and has been experimentally observed in platforms such as neutral atoms [9–11], ion traps [12], and superconducting qubits [13], with promising theoretical proposals in quantum algorithms, including quantum associative memory [14, 15] and quantum error correction [16].

Based on this concept, we show that if quantum hardware noise induces metastability, both digital and analog algorithms can be designed in a noise-aware fashion, achieving intrinsic resilience without requiring redundant encoding. This approach differs from conventional strategies, such as quantum error correction [17, 18] and decoherence-free subspaces [19, 20], which rely on adding extra qubits to encode information, introducing the experimental challenge of implementing non-transverse operations. While recent works have explored similar directions to tackling decoherence [21–25], a major limitation remains: existing methods lack an efficient way to compute a noise resilience metric. Typically, they require classical simulation of the quantum algorithm, preventing simultaneous evaluation of noise resilience and attainment of quantum advantage.

To address this shortcoming, we introduce a noise resilience measure that, under standard assumptions on the noise model, can be efficiently upper bounded for a wide class of algorithms without requiring full classical simulation. Moreover, in addition to presenting a general theoretical framework, we illustrate our theory with applications on well-known algorithms such as variational quantum algorithms [26, 27] and adiabatic state preparation [28, 29]. Importantly, our work extends beyond theoretical proposals—we present experimental evidence supporting the presence of metastable noise, for IBM's superconducting devices and D-Wave's quantum annealers [30]. These results suggest that metastability can be directly leveraged to enhance algorithmic performance on near-term quantum hardware.

II. METASTABILITY

In the context of dynamical systems, metastability refers to the emergence of intermediate, long-lived states resulting from the interplay of multiple dynamical timescales [4]. This phenomenon plays a central role in the dynamics of open quantum systems, which

^{*} sannia@ifisc.uib-csic.es

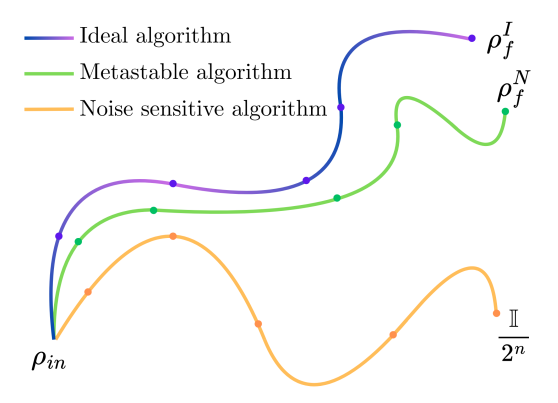


FIG. 1. Schematic illustration contrasting a noise-sensitive algorithm, whose final output approaches a fully mixed state, with a metastability-based algorithm, whose output remains close to the ideal target state. For different algorithms that give the same final state ρ_f^I , leveraging metastability allows selecting the one that, under noise conditions, prepares a final state ρ_f^N that is closer to the desired one.

we consider in the following [8]. Under the Markovian approximation, the general evolution of a density matrix ρ describing such a system is governed by the Gorini–Kossakowski–Lindblad–Sudarshan (GKLS) master equation [31–33]:

$$\frac{d\rho}{dt} = \mathcal{L}[\rho] \equiv -i[H, \rho] + \sum_{i} \gamma_{i} \left(L_{i} \rho L_{i}^{\dagger} - \frac{1}{2} \{ L_{i}^{\dagger} L_{i}, \rho \} \right)
= (\mathcal{U} + \mathcal{D})[\rho],$$
(1)

where H is the system Hamiltonian (generating the unitary superoperator \mathcal{U}), $\{L_i\}$ are the Lindblad (jump) operators modeling the coupling to the environment, and $\{\gamma_i\}$ are the associated decay rates. The dissipative contribution is collected in the superoperator \mathcal{D} .

Metastability in this setting is intimately connected to the spectral properties of the non-Hermitian Liouvillian superoperator \mathcal{L} . For a system of n qubits, and neglecting possible exceptional points [34], the Liouvillian can be diagonalized in a biorthogonal basis of left and right eigenmatrices, $\{\ell_i\}$ and $\{r_i\}$, such that

$$\mathcal{L}[r_j] = \lambda_j r_j, \quad \mathcal{L}^{\dagger}[\ell_j] = \lambda_j^* \ell_j, \quad \operatorname{Tr}\left(\ell_j^{\dagger} r_k\right) = \delta_{jk},$$

where all eigenvalues $\{\lambda_j\}$ satisfy $\operatorname{Re}(\lambda_j) \leq 0$ due to the contractivity of quantum channels.

For definiteness, suppose \mathcal{L} admits a unique stationary state ρ_{ss} with $\mathcal{L}[\rho_{ss}] = 0$. Then, any initial state $\rho(0)$ evolves as:

$$\rho(t) = \rho_{\rm ss} + \sum_{j\geq 1} e^{\lambda_j t} \operatorname{Tr}(\ell_j \rho(0)) r_j.$$
 (2)

All non-stationary contributions decay with time constants $\tau_j = 1/|\text{Re}(\lambda_j)|$, ultimately relaxing the system to

 $\rho_{\rm ss}$. When there is a clear separation in two timescales, for example, $\tau_1 \ll \tau_2$, metastability arises [8]. For times $\tau_1 \ll t \ll \tau_2$, the system appears nearly stationary. Its state is confined within a metastable manifold, spanned by those right eigenmatrices r_j whose corresponding eigenvalues fulfill $|\operatorname{Re}(\lambda_j)| \leq 1/\tau_2$.

Metastability also implies that different initial conditions $\rho(0)$ approach the stationary state $\rho_{\rm ss}$ at rates determined by the projection onto the various decay modes. Building on this structure, in the next sections, we illustrate how quantum algorithms can be adapted to exploit the metastable dynamics of noise, thereby enhancing their robustness.

III. NOISY QUANTUM CIRCUITS

A generic digital quantum algorithm can be described as a sequence of L layers of unitary gates U_k , typically implemented by a quantum circuit, applied to an initial state $\rho_{\rm in}$. The ideal, noiseless final state $\rho_f^{\rm ideal}$ is given by

$$\rho_f^{\text{ideal}} = \left(\prod_{k=1}^L U_k\right) \rho_{\text{in}} \left(\prod_{k=1}^L U_k\right)^{\dagger}.$$
 (3)

In practice, quantum circuits are affected by noise, which can be modeled by Markovian quantum channels represented as $e^{\mathcal{L}_k}$, where the evolution time is absorbed into the Liouvillian superoperator \mathcal{L}_k acting after each unitary. The resulting noisy final state ρ_f^{noisy} is thus

$$\rho_f^{\text{noisy}} = \prod_{k=1}^L e^{\mathcal{L}_k} \left[U_k \, \rho_{\text{in}} \, U_k^{\dagger} \right]. \tag{4}$$

We focus on the case where each channel $e^{\mathcal{L}_k}$ is unital, meaning that each \mathcal{L}_k preserves the maximally mixed state $\mathbb{I}/2^n$. This is relevant since, although nonunital noise can be exploited for specific algorithmic purposes [35–41], unital noise invariably drives ρ_f^{noisy} toward the trivial infinite-temperature state $\mathbb{I}/2^n$, thus erasing any useful information.

To analyze the effects of noise, we expand each \mathcal{L}_k in its eigenbasis: let $\{r_{i_k}^k\}_{i_k}$ denote the right eigenmatrices of \mathcal{L}_k and $\{\lambda_{i_k}^k\}_{i_k}$ their eigenvalues. Then the final noisy state of Eq. (4) can be written as

$$\rho_f^{\text{noisy}} = \frac{\mathbb{I}}{2^n} + \sum_{i_1, \dots, i_L} \alpha_{i_1}^1 \, \alpha_{i_1, i_2}^2 \cdots \alpha_{i_{L-1}, i_L}^L \, e^{\sum_{k=1}^L \lambda_{i_k}^k} \, r_{i_L}^L,$$
(5)

where the expansion coefficients are defined by $\rho_{\text{in}} = \sum_{i_1} \alpha_{i_1}^1 r_{i_1}^1$ and $U_k r_{i_{k-1}}^{k-1} U_k^{\dagger} = \sum_{i_k} \alpha_{i_{k-1},i_k}^k r_{i_k}^k$ for $k = 2, \ldots, L$.

The noiseless outcome ρ_f^{ideal} is immediately recovered by formally setting all exponential factors $e^{\sum_k \lambda_{i_k}^k} \to 1$ in Eq. (5). Consequently, given a set of noise generators $\{\mathcal{L}_k\}$, optimizing a quantum algorithm for noise resilience amounts to minimizing the decay associated with the exponential terms.

To assess an algorithm's resilience to noise, we introduce the index

$$\lambda_M = \min_{i_1, \dots, i_L} \operatorname{Re} \left\{ \sum_{k=1}^L \lambda_{i_k}^k \right\} \le 0, \tag{6}$$

so that greater values of λ_M correspond to better resilience against noise in the worst-case scenario. In fact, focusing on this quantity highlights the most vulnerable component of the dynamics, irrespective of the amplitude of its associated eigenvector. This approach fundamentally differs from other metrics in the literature that quantify the impact of decoherent noise [21, 22, 24], which, being based on fidelity calculations, require knowledge of the final state of the quantum algorithm. In contrast, the strength of our method lies in the fact that, as we show below, an upper bound to Eq. (6) can be computed for a broad class of algorithms without assuming the ability to simulate the quantum evolution, thereby preserving the possibility of a genuine quantum advantage

We note that while the set of eigenvalues $\lambda_{i_k}^k$ is fixed by the noise model, the exponents in Eq. (5) also depend on the specific algorithm, and the same holds for λ_M . Moreover, distinct algorithms can share the same minimum value of λ_M ; however, as will be discussed in the following section, counting how many times this minimum appears in the final state decomposition of Eq. (5) provides a way to discriminate their noise resilience. Furthermore, as illustrated in Fig. 1 and through subsequent examples, in the presence of metastability, certain algorithms correspond to significantly lower values of λ_M , leading to enhanced robustness to noise.

IV. VARIATIONAL QUANTUM ALGORITHMS

A. Noise-induced barren plateaus

We now demonstrate the application of our formalism to variational quantum algorithms (VQAs) [27], focusing specifically on mitigating noise-induced barren plateaus (NIBPs) [42]. In a VQA, the quantum circuit is controlled by a set of classical parameters. Following our established notation, each unitary layer U_k is a function of a parameter vector $\vec{\theta}_k$, such that $U_k = U_k(\vec{\theta}_k)$. All trainable parameters across the circuit are then aggregated into a single global vector $\vec{\theta}$. The goal of the algorithm is to optimize these parameters by minimizing a cost function. This function is typically the expectation value of a target observable O, and is thus expressed as $C(\vec{\theta}) = \text{Tr} \Big\{ O \rho_f(\vec{\theta}) \Big\}$, where $\rho_f(\vec{\theta})$ is the final state produced by the parameterized circuit.

The NIBP phenomenon poses a significant challenge to VQAs. It arises when noise in the circuit causes the gradient of the cost function, $\nabla C(\vec{\theta})$, to vanish exponentially with increasing circuit depth [43], namely the L layers.

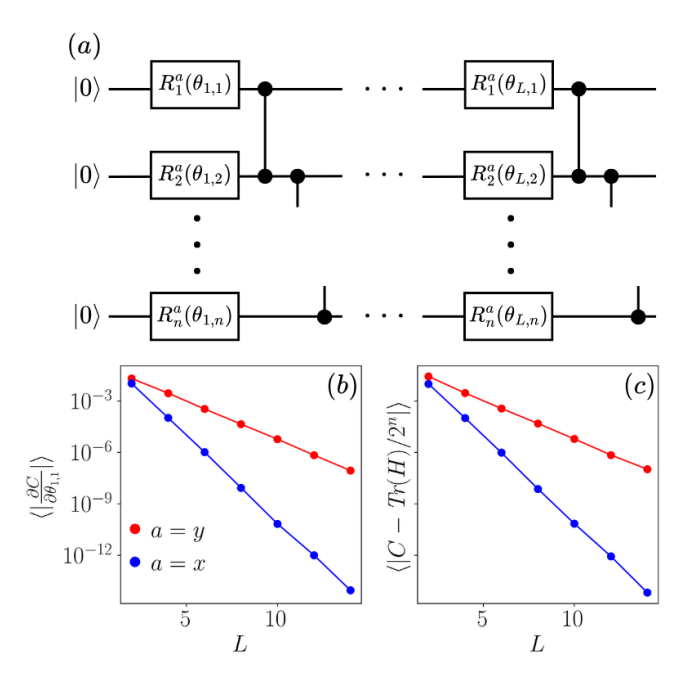


FIG. 2. (a) Ansatz used in the numerical simulations. (b) Absolute value of the cost-function derivative with respect to $\theta_{1,1}$. (c) Distance between the cost-function value obtained from the circuit output and the one relative to the fully mixed state. All the points are averages over 10^4 random circuit initializations. Noise parameters are fixed to $q_x = q_z = 0.5$, $q_y = 0$, taking n = 8. A significantly slower decay is found for the noise-adapted ansatz.

This occurs because the output state $\rho_f(\bar{\theta})$ is driven towards the maximally mixed state, erasing the landscape features necessary for optimization.

Our analytical framework provides a direct method for addressing this issue. The partial derivative of the cost function with respect to a single parameter $\theta_{k,l}$ (the *l*-th parameter in the *k*-th layer) is given by:

$$\frac{\partial C}{\partial \theta_{k,l}} = \sum_{i_1, \dots, i_L} \dots \frac{\partial \alpha_{i_{k-1}, i_k}^k}{\partial \theta_{k,l}} \dots e^{(\lambda_{i_1}^1 + \dots + \lambda_{i_L}^L)} \operatorname{Tr} \left\{ r_{i_L}^L O \right\}$$

The exponential decay characteristic of NIBPs is captured by the already studied terms $e^{(\sum_j \lambda_{i_j}^j)}$. Consequently, the introduced noise resilience index, λ_M , can also be directly connected to the gradient magnitude. In other terms, the parameterized circuits that minimize λ_M are also the ones that mitigate NIBPs the most.

B. Hardware-efficient ansatz example

To show our theory in a concrete example, we analyze the optimization of hardware-efficient ansatzes under local noise. As in Ref. [42], we model each circuit layer as the composition of local Pauli channels. After every unitary operation, the noise channel takes the form

$$e^{\mathcal{L}_k} = \bigotimes_{j=1}^n \mathcal{N}_j,\tag{7}$$

where the action of N_j on the j-th qubit is specified by

$$\mathcal{N}_{j}(\mathbb{I}) = \mathbb{I},$$

$$\mathcal{N}_{j}(\sigma_{j}^{a}) = q_{a}\sigma_{j}^{a},$$

with σ_j^a a Pauli operator on site j and parameters $-1 < q_x, q_y, q_z < 1$.

We focus on the anisotropic case where the y-direction is maximally affected by noise, i.e., $q_y = 0$. Inizialiting the system n qubits in $|\mathbf{0}\rangle$, we study two hardware-efficient variational circuits with building blocks

$$U_k = \prod_{i=1}^{n-1} CZ_{i,i+1} \circ \prod_{i=1}^n R_i^a(\theta_{k,i}),$$
 (8)

where $CZ_{i,i+1}$ is a controlled-Z gate between qubits i and i+1, and $R_i^a(\theta_{k,i})$ is a single-qubit rotation of qubit i around axis a [see Fig. 2 (a) for a representation].

For the chosen initial condition, only the two directions a=x and a=y yield non-trivial outputs. An analysis of the final state Pauli string decomposition for these two cases shows that, for both ansatzes, λ_M saturates its lower bound: $\lambda_M \to -\infty$. However, as discussed in the Supplemental Material, when a=y, the number of final right eigenvectors corresponding to this minimum is significantly smaller, making this ansatz noise-adapted according to our noise resilience index.

For our numerical analysis, as the cost Hamiltonian, we take $H = \sigma_1^z \sigma_2^z$, and compute both the cost-function derivative and its deviation from the fully mixed state value, $C = \text{Tr}(H)/2^n$. As shown in Fig. 2, both quantities decay exponentially with the number of layers L, confirming the emergence of noise-induced barren plateaus. Importantly, the decay is substantially slower for the noise-aware circuit, demonstrating that such ansatzes allow for an exponentially larger circuit depth at fixed measurement resources.

V. EXPERIMENTAL NOISE BENCHMARK IN THE IBM MACHINE

Given the framework presented above, the question arises as to whether this could be leveraged in a current quantum device. To this end, using the same class of circuits of Eq. (8) and the same target Hamiltonian $H = \sigma_1^z \sigma_2^z$, we repeated the analysis previously made, implementing the circuits on the 156 qubits ibm_fez device. For each realization, we estimated the observable expectation value using 10000 shots. As shown in Fig. 3, while in the ideal case both circuits take the same average cost function distance from the one evaluated on the fully mixed state, the results on the real device show a clear

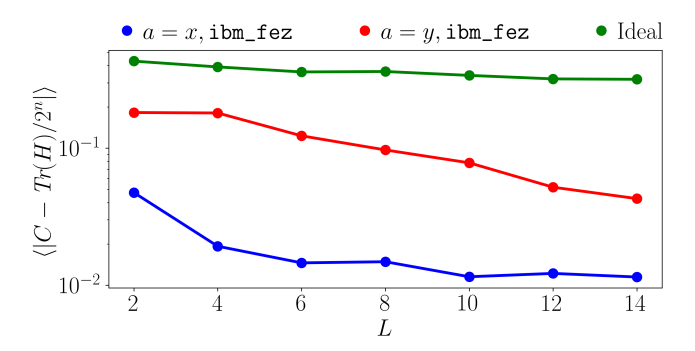


FIG. 3. Difference between the observable expectation values evaluated on the circuits implemented on the ibm_fez device and the one theoretically evaluated on the fully mixed state. Each point has been averaged on 100 random circuit initializations, while each sample is estimated using 10000 shots. The number of the considered device lines used for building both circuits is n=12. The green line represents the ideal average distance, which coincides for both circuits.

difference for the two different symmetries. In particular, we observe that the case a=y appears to be more noise resilient, as in the numerical example above. Moreover, we note that the expected exponential decay has not been fully reproduced in the case of a=x. We explain this behavior by noting that, given the limited budget in terms of the number of available measurements, the cost function values can be evaluated only up to a precision of the order of 10^{-2} . Consequently, once the computed difference approaches this limit, we do not have enough experimental resolution to keep reproducing the decay.

VI. UPPER BOUND ON THE NOISE RESILIENCE OF QUANTUM CIRCUITS

A complete characterization of the noise affecting a quantum circuit generally requires an exponentially large number of resources. However, in practice, efficient techniques exist that approximate noise models well, requiring only polynomial resources in the number of qubits. In particular, methods based on Pauli twirling, using Pauli decompositions, provide compact approximate representations of the effective noise channels $e^{\mathcal{L}_k}$ in Eq. (4) [44–48]:

$$e^{\mathcal{L}_k}[\rho] = (1 - \sum_{i=1}^{N_k} p_{k,i})\rho + \sum_{i=1}^{N_k} p_{k,i} \,\mathcal{P}_{k,i}^{(N)}[\rho]\mathcal{P}_{k,i}^{(N)}, \qquad (9)$$

where ρ is a density matrix, $\mathfrak{P}_{k,i}^{(N)}$ denotes a Pauli string, $p_{k,i}$ is its corresponding weight belonging to the set (0,1], and $N_k = \mathcal{O}(\text{poly}(n))$.

This decomposition enables the efficient computation of a noise resilience upper bound, $\tilde{\lambda}_M$, for a broad class of quantum algorithms, giving resources that are sufficient to read the circuit output. Assuming that the input state $\rho_{\rm in}$ is a stabilizer state, we consider algorithms

implemented by a layered sequence of Clifford operations $U_{c,k}$ interleaved with non-Clifford gates $U_{nc,k}$, where we assume that the latter do not change the set of Pauli strings that generate the qubits state at each layer, like in the already presented hardware-efficient ansatz example. This implies that the Pauli operators belonging to this set can be efficiently computed at each stage of the algorithm [49, 50]. Importantly, this does not mean that the outcome of the algorithm can be efficiently determined, due to the presence of non-Clifford operations that make simulating the circuit harder in a classical setting.

The procedure for upper-bounding the noise resilience can be summarized as follows:

Algorithm 1 Computation of an upper bound to noise resilience

 $\begin{array}{|c|c|c|} \hline \textbf{Require:} & \rho_{\text{in}} & \rhd \text{Initial stabilizer state} \\ \hline \textbf{Require:} & \{U_{c,k}\} & \rhd \text{Set of Clifford gates} \\ \hline \textbf{Require:} & \{\mathcal{P}_{k,i}^{(N)}\}_{k,i} & \rhd \text{Noise Pauli strings} \\ \hline \textbf{Require:} & \{p_{k,i}\}_{k,i} & \rhd \text{Associated Pauli weights} \\ \hline \textbf{Ensure:} & \tilde{\lambda}_M & \rhd \text{Upper bound for noise resilience} \\ \hline 1: & \text{Compute Pauli decomposition of } \rho_{\text{in}} : \\ \hline \end{array}$

$$\rho_{\rm in} \to \{\mathcal{P}_{0,i}^{(S)}\}$$

- 2: Initialize: $\tilde{\lambda}_M \leftarrow 0$
- 3: for k = 1 to L do
- 4: Update state decomposition under Clifford action:

$$\{\mathcal{P}_{k+1,i}^{(S)}\} \leftarrow U_{c,k+1} \{\mathcal{P}_{k,i}^{(S)}\} U_{c,k+1}^{\dagger}$$

- 5: Match each $\mathcal{P}_{k+1,i}^{(S)}$ with its corresponding Pauli noise coefficient $p_{k,i}$
- 6: Update:

$$\tilde{\lambda}_M \leftarrow \tilde{\lambda}_M + \min_i \log \left(1 - \sum_{i=1}^{N_k} p_{k,i} + p_{k,i}\right)$$

- 7: end for
- 8: return $\tilde{\lambda}_M$

An important observation is that this procedure is entirely independent of the non-Clifford layers in the circuit, and this independence underlies its efficiency.

VII. ANALOG QUANTUM ALGORITHMS

In addition to the class of digital algorithms described in the previous sections, our framework can be adapted to an analog scenario. In this case, we consider the algorithm to be implemented by a time-dependent Hamiltonian H(t), such that:

$$\rho_f^I = U(t)\rho_{\rm in}U(t)^{\dagger},\tag{10}$$

with

$$U(t) = \Im e^{\int_0^T H(t)dt},\tag{11}$$

where T is the total algorithm execution time and \Im is the time-ordering operation.

In a noisy regime, H(t) is replaced by time dependent Liouvillian $\mathcal{L}(t)$, which gives

$$\rho_f^N = \Im e^{\int_0^T \mathcal{L}(t)dt} [\rho_{\rm in}]. \tag{12}$$

In this continuous limit, our strategy translates to minimizing the contributions of the dissipative term $\mathcal{D}(t)[\rho(t)]$ during the system evolution.

A. Noise resilience upper bound in the continuous case

As in the previous case, it is possible, under similar hypotheses, to efficiently compute a noise resilience upper bound also in this analog case. As before, we assume to have a Pauli noise model for the dissipator:

$$\mathcal{D}(t)[\mathcal{P}_i] = p_i(t)\mathcal{P}_i$$

where \mathcal{P}_i is generic Pauli string and $p_i(t)$ is a real number such that |p(t)| < 1.

Moreover, as in the previously analyzed digital context, we assume that without fully knowing the action of H(t), we can still efficiently access the Pauli strings present in the system state decomposition at each time. This translates to knowing a function $g_i(t)$ such that:

$$g_i(t) = \begin{cases} 0, & \text{if } \operatorname{Tr}[\rho(t)\mathcal{P}_i] = 0, \\ 1, & \text{otherwise.} \end{cases}$$

Given this setup, an upper bound on the noise resilience is given by:

$$\tilde{\lambda}_M = \int_0^T \max_i (g_i(t)p_i(t))dt. \tag{13}$$

Moreover, as we will show in the examples below, understanding which is the algorithm that minimizes Eq. (13) does not always require a computation of $\tilde{\lambda}_M$.

B. Single-qubit analytical example

We now illustrate our framework with a simple singlequbit example. Consider an analog algorithm designed to implement a bit-flip operation such that

$$|1\rangle = U(T)|0\rangle, \tag{14}$$

with U(t) a unitary rotation about either the x- or y-axis of the Bloch sphere and total evolution time $T=\pi$.

The effect of noise is modeled by a Lindblad superoperator of the form

$$\mathcal{D} = \gamma_x \mathcal{D}_x + \gamma_y \mathcal{D}_y + \gamma_z \mathcal{D}_z, \tag{15}$$

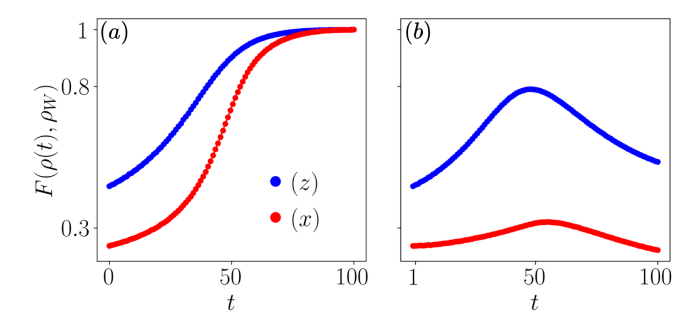


FIG. 4. Fidelity evolution over time for the Adiabatic State Preparation example. (a) Noiseless case. (b) Noisy case. The total evolution time is fixed at T=100, and the system size is n=5.

where \mathcal{D}_a denotes the dissipator associated with the jump operator σ^a ($a \in \{x, y, z\}$).

Assume now that $\gamma_x \gg \gamma_y, \gamma_z = \epsilon$. A straightforward analytical calculation shows that the two different choices of rotation axis lead to substantially different fidelities with respect to the target state. Denoting by $\rho_{f,x}^N$ and $\rho_{f,y}^N$ the noisy final states obtained from x- and y-axis rotations, respectively, we find

$$\rho_{f,x}^{N} = \mathbb{I} - e^{-(\gamma_x + \epsilon)T} \sigma^z \simeq \mathbb{I} - e^{-\gamma_x T} \sigma^z,$$

$$\rho_{f,y}^{N} = \mathbb{I} - e^{-2\epsilon T} \sigma^z.$$

Since the target state can be written as

$$|1\rangle\langle 1| = \mathbb{I} - \sigma^z,\tag{16}$$

we conclude that a noisy rotation about the y axis yields a final state significantly closer to the desired target state. In other words, under this anisotropic noise model dominated by σ^x errors, the y-axis rotation constitutes the more resilient strategy.

VIII. ADIABATIC STATE PREPARATION

As a richer example, we now consider another algorithm belonging to this class: adiabatic state preparation [28, 29]. This method relies on the adiabatic theorem, which guarantees that a quantum system initially in the ground state $|\psi_0\rangle$ of a simple Hamiltonian H_0 will remain close to the ground state of a changing H_s if such a change is slow enough. By defining H_f as the final Hamiltonian, whose ground state coincides with the desired target state, the algorithm prepares such a state by evolving $|\psi_0\rangle$ for a sufficiently long time T under the time-dependent Hamiltonian

$$H(s) = A(s)H_0 + B(s)H_f.$$
 (17)

Here, s = s(t) satisfies s(0) = 0 and s(T) = 1. The interpolation functions A(s) and B(s) are chosen so that $A(0)/B(0) \gg 1$ and $A(1)/B(1) \ll 1$, ensuring a smooth transition from H_0 to H_f .

As a concrete instance, we focus on preparing the n-qubit W state [51–53]

$$|W\rangle = \frac{1}{\sqrt{n}} \sum_{i=1}^{n} |e_i\rangle, \qquad (18)$$

where $|e_i\rangle$ denotes the computational basis state with all qubits in $|0\rangle$ except the *i*-th one, which is in $|1\rangle$. This state can be obtained adiabatically by taking the target Hamiltonian

$$H_f = -\sum_{i \neq j} |e_i\rangle \langle e_j|,$$

whose ground state is, precisely, $|W\rangle$. We study two different initial conditions:

$$(z): H_{0,z} = \sigma_1^z - \sum_{i=2}^n \sigma_i^z, \qquad |\psi_{0,z}\rangle = |e_1\rangle,$$

$$(x): H_{0,x} = \sigma_1^x - \sum_{i=2}^n \sigma_i^x, \quad |\psi_{0,x}\rangle = \prod_{i=1}^n R_i^y(\pi/2) |e_1\rangle.$$

Following the previous methodology, we now examine how these two approaches respond to noise of the form given in Eq. (15). Specifically, we choose

$$\gamma_z = \sqrt{1/T}, \quad \gamma_x = \gamma_y = 0,$$

and we interpolate linearly between H_0 and H_f with A(s) = 1 - s and B(s) = s.

Figure 4(a) shows the fidelity between the time-evolved state $\rho(t)$ and the target state $\rho_W = |W\rangle \langle W|$ in the ideal noiseless case. Both initial conditions succeed, achieving final fidelities $F \simeq 1$. However, the situation changes dramatically in the presence of noise, as seen in Fig. 4(b). For the (z) initialization, fidelities as high as $F \simeq 0.8$ remain achievable, while in the (x) initialization the maximum fidelity drops to $F \simeq 0.3$.

This difference can be understood by noting that, in the (z) case, the Pauli decomposition of $\rho(t)$ predominantly consists of strings commuting with σ^z , rendering them largely unaffected by the chosen noise channel. In contrast, the (x) case introduces components sensitive to the noise, leading to stronger degradation. Additionally, at long times, a fidelity decay is observed in both cases due to relaxation toward a stationary state imposed by the noise, which generally does not coincide with the target state. Hence, in noisy conditions, one must strike a balance between total runtime T and final state accuracy.

IX. EXPERIMENTAL NOISE BENCHMARK IN THE D-WAVE MACHINES

Analogously to the case of digital algorithms, we now turn to the analog setting and experimentally verify that metastability effects can also be observed in analog quantum processors. In particular, we focus on D-Wave's

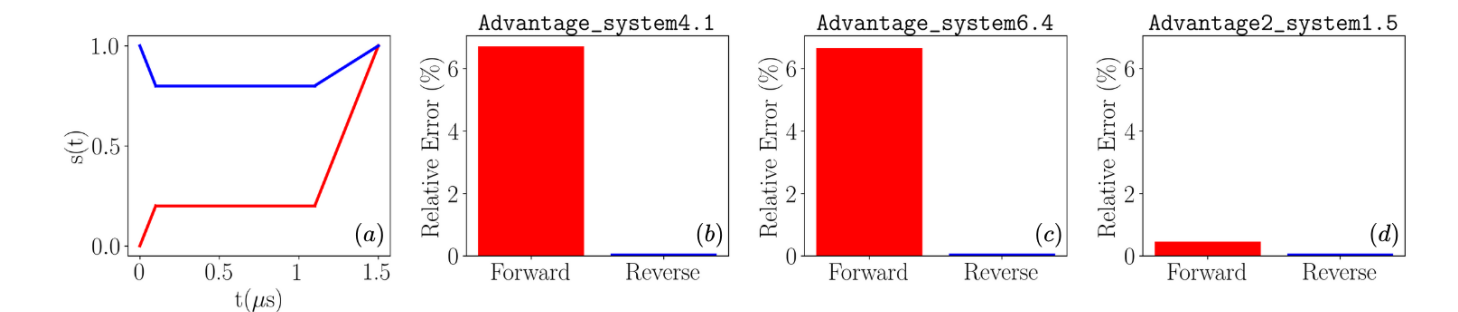


FIG. 5. (a) Annealing schedules implemented in the D-Wave devices. The forward protocol is shown in red, while the reverse protocol is in blue. (b-d) Relative errors between the experimentally measured average energy and the theoretically expected value for the Advantage_system4.1, Advantage_system6.4, and Advantage2_system1.5 machines, respectively. Each experimental point is computed taking 1000 samples. Statistical uncertainties were found to be negligible.

quantum annealing devices [30], which have been used to study both classical as well as quantum spin systems extensively [54–56].

We implement quantum annealing experiments on three QPUs spanning two generations of annealers. For each device, the methodology is as follows: we partition the hardware into two-qubit subsystems, consistent with the native chip connectivity, and apply the same annealing protocol to every pair. This allows us to extract an averaged error profile across the full processor. To probe the role of algorithmic symmetry, we vary the annealing schedule while fixing the target Hamiltonian

$$H_f = -0.1(\sigma_1^z + \sigma_2^z) - \sigma_1^z \sigma_2^z.$$

We first analyze the standard forward annealing protocol, where the schedule s(t) remains close to zero for most of the evolution, as shown in the red line of Fig. 5 (a). On D-Wave platforms, every forward anneal starts with

$$H_0 = -\left(\sigma_1^x + \sigma_2^x\right), \qquad |\psi_0\rangle = |+\rangle^{\otimes 2}.$$

Hence, during most of the dynamics, the Pauli decomposition of the state is dominated by strings symmetric under the σ_i^x operators.

As a complementary protocol, we consider reverse annealing, where the schedule starts at s(0)=1 and $H_0=H_f$. In this case, we initialize the system in the known ground state of the target Hamiltonian to obtain similar final states for both schedules. Here, s(t) remains close to one, and the system state predominantly exhibits symmetry under the σ_i^z operators, as depicted by the blue line of Fig. 5(a).

To quantify device-induced deviations, we compute the relative error

$$\mathrm{R.E.(\%)} = 100 \times \frac{E_{\mathrm{exp}} - \bar{E}}{\bar{E}},$$

where E_{exp} is the experimentally measured average energy and E is the theoretically expected energy, obtained from a closed-system classical simulation. To compute

E, we implement classical simulations of closed quantum evolutions corresponding to the protocols considered using the QuantumAnnealing.jl package [57]. For all cases, we find that $\bar{E} \simeq -1.2$, i.e., the final energy coincides with the ground state energy of H_f . While our implementations are well within the adiabatic regime, we observe small deviations from the ground state energy, which arise due to the anneal ramps at the beginning and end of the protocols.

The experimental results in Fig. 5 reveal a systematic asymmetry. For reverse annealing, experimental and theoretical values coincide within numerical precision, yielding vanishing relative errors across all platforms. By contrast, forward annealing shows non-negligible errors, although the magnitude of these decreases on newer generations of hardware, with the Advantage2_system1.5 device achieving the closest agreement with ideal predictions.

Taken together, these observations support the interpretation that noise asymmetries in D-Wave processors primarily affect states symmetric with respect to the σ_i^x operators. It is worth noting that, in general, the noise models used to describe the behavior of D-Wave machines lead to system thermalization [58–60] in the time regimes considered (of the order of a few hundred microseconds). This implies that the decoherence channels related to these platforms are non-unital, in contrast to those considered in our theoretical framework. Importantly, this example demonstrates that our study of metastable behavior can be naturally extended to the non-unital noise setting, although a detailed investigation of these aspects is left for future work. Finally, we emphasize that the noise symmetries identified in our analysis are consistent with previous studies performed in different regimes [59, 60], thereby supporting the broader generality of this property.

X. CONCLUSIONS

In this work, we have established a novel approach for witnessing noise in quantum algorithms by leveraging the phenomenon of metastability in open quantum systems. Our results demonstrate that when quantum hardware noise exhibits metastable dynamics, both digital and analog algorithms can be designed to achieve intrinsic resilience by aligning algorithmic symmetries with the noise structure, without the need for redundant encoding such as in standard quantum error correction.

We provided a general theoretical framework, introduced a practical noise resilience metric that avoids the need for classical simulation of the full algorithm, and illustrated our approach through applications to variational quantum algorithms and analog adiabatic state preparation. Importantly, we validated the relevance of our framework with experimental benchmarks on IBM superconducting processors and D-Wave annealers, confirming that metastable noise effects are present and can be systematically exploited to improve algorithmic outcomes on currently available hardware.

Our findings suggest that the structured properties of noise in quantum devices can serve as a direct algorithmic resource, and open new directions for noise-aware algorithm design. This paradigm enables meaningful progress towards robust quantum computation in the NISQ era, bridging theoretical developments and experimental practice. Future work may focus on further characterizing metastability across platforms and extending these concepts to more general noise models that, for example, exhibit features of non-Markovianity.

ACKNOWLEDGEMENTS

The authors acknowledge Davide Venturelli for useful dicussions. A. S. acknowledges the Span-

ish State Research Agency, through the María de Maeztu project CEX2021-001164-M funded by the MCIU/AEI/10.13039/501100011033, through the CO-QUSY project PID2022-140506NB-C21 and -C22 funded MCIU/AEI/10.13039/501100011033, MINECO through the QUANTUM SPAIN project, and EU through the RTRP - NextGenerationEU within the framework of the Digital Spain 2025 Agenda. also acknowledges the CSIC Interdisciplinary Thematic Platform (PTI+) on Quantum Technologies in Spain (QTEP+) and the support of a fellowship from the "la Caixa" Foundation (ID 100010434 -LCF/BQ/DI23/11990081). A. S. also acknowledges support from the U.S. Department of Energy (DOE) through a quantum computing program sponsored by the Los Alamos National Laboratory (LANL) Information Science & Technology Institute. A.S. has also been supported by the USRA Feynman Quantum Academy internship program. P.S. acknowledge the support of NNSA for the U.S. DOE at LANL under Contract No. DE-AC52-06NA25396, and Laboratory Directed Research and Development (LDRD) for support through 20240032DR. L.P.G.P. acknowledges support from the Beyond Moore's Law project of the Advanced Simulation and Computing Program at LANL, and the DOE Office of Advanced Scientific Computing Research, Accelerated Research for Quantum Computing program, Fundamental Algorithmic Research toward Quantum Utility (FAR-Qu) project. We would also like to thank the New Mexico Consortium, under subcontract C2778, the Quantum Cloud Access Project (QCAP), for providing quantum computing resources and technical collaboration.

^[1] J. Preskill, Quantum Computing in the NISQ era and beyond, Quantum 2, 79 (2018).

^[2] D. Stilck França and R. García-Patrón, Limitations of optimization algorithms on noisy quantum devices, Nat. Phys. 17, 1221–1227 (2021).

^[3] Z. Cai, R. Babbush, S. C. Benjamin, S. Endo, W. J. Huggins, Y. Li, J. R. McClean, and T. E. O'Brien, Quantum error mitigation, Rev. Mod. Phys. 95, 045005 (2023).

^[4] B. A. W. Brinkman, H. Yan, A. Maffei, I. M. Park, A. Fontanini, J. Wang, and G. La Camera, Metastable dynamics of neural circuits and networks, Applied Physics Reviews 9, 10,1063/5,0062603 (2022).

^[5] J. Langer, Statistical theory of the decay of metastable states, Annals of Physics 54, 258–275 (1969).

^[6] P. Hänggi, P. Talkner, and M. Borkovec, Reaction-rate theory: fifty years after Kramers, Rev. Mod. Phys. 62,

^{251-341 (1990).}

^[7] E. Tognoli and J. A. S. Kelso, The metastable brain, Neuron 81, 35–48 (2014).

^[8] K. Macieszczak, M. Guţă, I. Lesanovsky, and J. P. Garrahan, Towards a theory of metastability in open quantum dynamics, Phys. Rev. Lett. 116, 240404 (2016).

^[9] Y. Wu, S. Kolkowitz, S. Puri, and J. D. Thompson, Erasure conversion for fault-tolerant quantum computing in alkaline earth Rydberg atom arrays, Nat. Commun. 13, 10.1038/s41467-022-32094-6 (2022).

^[10] N. Chen, L. Li, W. Huie, M. Zhao, I. Vetter, C. H. Greene, and J. P. Covey, Analyzing the Rydberg-based optical-metastable-ground architecture for ¹⁷¹Yb, Phys. Rev. A 105, 10.1103/PhysRevA.105.052438 (2022).

^[11] S. Darbha, M. Kornjača, F. Liu, J. Balewski, M. R. Hirsbrunner, P. L. S. Lopes, S.-T. Wang, R. Van Beeu-

- men, K. Klymko, and D. Camps, Long-lived oscillations of metastable states in neutral atom systems, Physi. Rev. B **110**, 10.1103/physrevb.110.155114 (2024).
- [12] D. T. C. Allcock, W. C. Campbell, J. Chiaverini, I. L. Chuang, E. R. Hudson, I. D. Moore, A. Ransford, C. Roman, J. M. Sage, and D. J. Wineland, omg blueprint for trapped ion quantum computing with metastable states, App. Phys. Lett. 119, 10.1063/5.0069544 (2021).
- [13] X. Shi, J. Sinanan-Singh, K. DeBry, S. L. Todaro, I. L. Chuang, and J. Chiaverini, Long-lived metastable-qubit memory, Phys. Rev. A 111, L020601 (2025).
- [14] A. Labay-Mora, R. Zambrini, and G. L. Giorgi, Quantum associative memory with a single driven-dissipative nonlinear oscillator, Phys. Rev. Lett. 130, 190602 (2023).
- [15] A. Labay-Mora, E. Fiorelli, R. Zambrini, and G. L. Giorgi, Theoretical framework for quantum associative memories, Quantum Sci. Technol. 10, 035050 (2025).
- [16] T. Botzung and E. Fiorelli, Error recovery protocols within metastable decoherence-free subspaces (2025), arXiv:2506.19631 [quant-ph].
- [17] D. A. Lidar and T. A. Brun, Quantum error correction (Cambridge university press, 2013).
- [18] B. M. Terhal, Quantum error correction for quantum memories, Rev. Mod. Phys. 87, 307 (2015).
- [19] D. A. Lidar, I. L. Chuang, and K. B. Whaley, Decoherence-free subspaces for quantum computation, Phys. Rev. Lett. 81, 2594 (1998).
- [20] D. A. Lidar, Review of decoherence-free subspaces, noiseless subsystems, and dynamical decoupling, Quantum Information and Computation for Chemistry , 295–354 (2014).
- [21] N. Funcke and J. Berberich, Robustness of optimal quantum annealing protocols, New Journal of Physics 26, 093040 (2024).
- [22] L. P. García-Pintos, T. O'Leary, T. Biswas, J. Bringewatt, L. Cincio, L. T. Brady, and Y.-K. Liu, Resilience—runtime tradeoff relations for quantum algorithms, Rep. Prog. Phys. 88, 037601 (2025).
- [23] J. Berberich, D. Fink, and C. Holm, Robustness of quantum algorithms against coherent control errors, Phys. Rev. A 109, 012417 (2024).
- [24] J. Berberich, T. Fellner, R. L. Kosut, and C. Holm, Robustness of quantum algorithms: Worst-case fidelity bounds and implications for design (2025), arXiv:2509.08481 [quant-ph].
- [25] J. Zeng and X.-H. Deng, Fundamental costs of noiserobust quantum control: Speed limits and complexity (2025), arXiv:2510.07183 [quant-ph].
- [26] A. Peruzzo, J. McClean, P. Shadbolt, M.-H. Yung, X.-Q. Zhou, P. J. Love, A. Aspuru-Guzik, and J. L. O'Brien, A variational eigenvalue solver on a photonic quantum processor, Nat. Commun. 5, 10.1038/ncomms5213 (2014).
- [27] M. Cerezo, A. Arrasmith, R. Babbush, S. C. Benjamin, S. Endo, K. Fujii, J. R. McClean, K. Mitarai, X. Yuan, L. Cincio, and P. J. Coles, Variational quantum algorithms, Nature Reviews Physics 3, 625–644 (2021).
- [28] E. Farhi, J. Goldstone, S. Gutmann, and M. Sipser, Quantum computation by adiabatic evolution (2000).
- [29] T. Albash and D. A. Lidar, Adiabatic quantum computation, Rev. Mod. Phys. 90, 10.1103/RevMod-Phys.90.015002 (2018).
- [30] M. W. Johnson, M. H. S. Amin, S. Gildert, T. Lanting, F. Hamze, N. Dickson, R. Harris, A. J. Berkley, J. Johansson, P. Bunyk, E. M. Chapple, C. Enderud,

- J. P. Hilton, K. Karimi, E. Ladizinsky, N. Ladizinsky, T. Oh, I. Perminov, C. Rich, M. C. Thom, E. Tolkacheva, C. J. S. Truncik, S. Uchaikin, J. Wang, B. Wilson, and G. Rose, Quantum annealing with manufactured spins, Nature 473, 194 (2011).
- [31] H.-P. Breuer, F. Petruccione, et al., The theory of open quantum systems (Oxford University Press on Demand, 2002).
- [32] V. Gorini, A. Kossakowski, and E. C. G. Sudarshan, Completely positive dynamical semigroups of n-level systems, J. Math. Phys. 17, 821 (1976).
- [33] G. Lindblad, On the generators of quantum dynamical semigroups, Commun. Math. Phys. 48, 119 (1976).
- [34] F. Minganti, A. Miranowicz, R. W. Chhajlany, and F. Nori, Quantum exceptional points of non-hermitian Hamiltonians and Liouvillians: The effects of quantum jumps, Phys. Rev. A 100, 062131 (2019).
- [35] S. Diehl, A. Micheli, A. Kantian, B. Kraus, H. P. Büchler, and P. Zoller, Quantum states and phases in driven open quantum systems with cold atoms, Nat. Phys. 4, 878–883 (2008).
- [36] F. Verstraete, M. M. Wolf, and J. Ignacio Cirac, Quantum computation and quantum-state engineering driven by dissipation, Nat. Phys. 5, 633–636 (2009).
- [37] P. M. Harrington, E. J. Mueller, and K. W. Murch, Engineered dissipation for quantum information science, Nature Reviews Physics 4, 660–671 (2022).
- [38] A. Sannia, R. Martínez-Peña, M. C. Soriano, G. L. Giorgi, and R. Zambrini, Dissipation as a resource for Quantum Reservoir Computing, Quantum 8, 1291 (2024).
- [39] A. Sannia, F. Tacchino, I. Tavernelli, G. L. Giorgi, and R. Zambrini, Engineered dissipation to mitigate barren plateaus, npj Quantum Inf. 10, 10.1038/s41534-024-00875-0 (2024).
- [40] X. Mi et al., Stable quantum-correlated many-body states through engineered dissipation, Science 383, 1332 (2024).
- [41] F. B. Maciejewski, J. Biamonte, S. Hadfield, and D. Venturelli, Improving quantum approximate optimization by noise-directed adaptive remapping (2024), arXiv:2404.01412 [quant-ph].
- [42] S. Wang, E. Fontana, M. Cerezo, K. Sharma, A. Sone, L. Cincio, and P. J. Coles, Noise-induced barren plateaus in variational quantum algorithms, Nat. Commun. 12, 10.1038/s41467-021-27045-6 (2021).
- [43] M. Larocca, S. Thanasilp, S. Wang, K. Sharma, J. Biamonte, P. J. Coles, L. Cincio, J. R. McClean, Z. Holmes, and M. Cerezo, Barren plateaus in variational quantum computing, Nature Reviews Physics 7, 174–189 (2025).
- [44] J. Emerson, M. Silva, O. Moussa, C. Ryan, M. Laforest, J. Baugh, D. G. Cory, and R. Laflamme, Symmetrized characterization of noisy quantum processes, Science 317, 1893–1896 (2007).
- [45] E. Magesan, J. M. Gambetta, and J. Emerson, Scalable and robust randomized benchmarking of quantum processes, Phys. Rev. Lett. 106, 180504 (2011).
- [46] Z. Cai and S. C. Benjamin, Constructing smaller pauli twirling sets for arbitrary error channels, Sci. Rep. 9, 10.1038/s41598-019-46722-7 (2019).
- [47] A. Erhard, J. J. Wallman, L. Postler, M. Meth, R. Stricker, E. A. Martinez, P. Schindler, T. Monz, J. Emerson, and R. Blatt, Characterizing large-scale quantum computers via cycle benchmarking, Nat. Com-

- $mun. \ \, \textbf{10}, \ 10.1038/s41467\text{-}019\text{-}13068\text{-}7 \ (2019).$
- [48] E. Magesan et al., Efficient measurement of quantum gate error by interleaved randomized benchmarking, Phys. Rev. Lett. 109, 080505 (2012).
- [49] D. Gottesman, The Heisenberg representation of quantum computers (1998), arXiv:quant-ph/9807006 [quant-ph].
- [50] S. Aaronson and D. Gottesman, Improved simulation of stabilizer circuits, Phys. Rev. A 70, 052328 (2004).
- [51] W. Dür, G. Vidal, and J. I. Cirac, Three qubits can be entangled in two inequivalent ways, Phys. Rev. A 62, 062314 (2000).
- [52] A. Cabello, Bell's theorem with and without inequalities for the three-qubit Greenberger-Horne-Zeilinger and W states, Phys. Rev. A 65, 032108 (2002).
- [53] P. Agrawal and A. Pati, Perfect teleportation and superdense coding with w states, Phys. Rev. A 74, 062320 (2006).
- [54] P. Kairys, A. D. King, I. Ozfidan, K. Boothby, J. Raymond, A. Banerjee, and T. S. Humble, Simulating the Shastry-Sutherland Ising Model Using Quantum Annealing, PRX Quantum 1, 020320 (2020).
- [55] A. D. King, C. Nisoli, E. D. Dahl, G. Poulin-Lamarre, and A. Lopez-Bezanilla, Qubit spin ice, Science 373, 576 (2021).
- [56] A. D. King, A. Nocera, M. M. Rams, J. Dziarmaga, R. Wiersema, W. Bernoudy, J. Raymond, N. Kaushal, N. Heinsdorf, R. Harris, K. Boothby, F. Altomare,

- M. Asad, A. J. Berkley, M. Boschnak, K. Chern, H. Christiani, S. Cibere, J. Connor, M. H. Dehn, R. Deshpande, S. Ejtemaee, P. Farre, K. Hamer, E. Hoskinson, S. Huang, M. W. Johnson, S. Kortas, E. Ladizinsky, T. Lanting, T. Lai, R. Li, A. J. R. MacDonald, G. Marsden, C. C. McGeoch, R. Molavi, T. Oh, R. Neufeld, M. Norouzpour, J. Pasvolsky, P. Poitras, G. Poulin-Lamarre, T. Prescott, M. Reis, C. Rich, M. Samani, B. Sheldan, A. Smirnov, E. Sterpka, B. T. Clavera, N. Tsai, M. Volkmann, A. M. Whiticar, J. D. Whittaker, W. Wilkinson, J. Yao, T. J. Yi, A. W. Sandvik, G. Alvarez, R. G. Melko, J. Carrasquilla, M. Franz, and M. H. Amin, Beyond-classical computation in quantum simulation, Science (2025).
- [57] Z. Morrell, M. Vuffray, S. Misra, and C. Coffrin, QuantumAnnealing: A Julia Package for Simulating Dynamics of Transverse Field Ising Models (2024), arXiv:2404.14501.
- [58] J. Marshall, E. G. Rieffel, and I. Hen, Thermalization, freeze-out, and noise: Deciphering experimental quantum annealers, Phys. Rev. Appl. 8, 064025 (2017).
- [59] J. Marshall, D. Venturelli, I. Hen, and E. G. Rieffel, Power of pausing: Advancing understanding of thermalization in experimental quantum annealers, Phys. Rev. Appl. 11, 044083 (2019).
- [60] Z. Morrell, M. Vuffray, A. Y. Lokhov, A. Bärtschi, T. Albash, and C. Coffrin, Signatures of open and noisy quantum systems in single-qubit quantum annealing, Phys. Rev. Appl. 19, 034053 (2023).

SUPPLEMENTAL MATERIAL FOR "UNCOVERING AND CIRCUMVENTING NOISE IN QUANTUM ALGORITHMS VIA METASTABILITY"

I. NOISE RESILIENCE FOR THE HARDWARE-EFFICIENT ANSATZ EXAMPLE

We now proceed to evaluate the noise resilience of the hardware-efficient ansatzes introduced in the main text. Importantly, as required, this calculation does not require knowing the corresponding circuit final states. For the considered noise model, described by Eq. (7) in the main text, the left and right eigenvectors of the noise superoperator coincide and correspond to the set of Pauli strings. Moreover, the minimum value of the noise-resilience index, λ_M , diverges to $-\infty$ whenever the noise channel acts on Pauli strings containing at least one σ_y matrix. Consequently, identifying the most noise-resilient ansatz reduces to counting the number of Pauli strings that contain a σ_y operator at each layer of the circuit.

Let us first consider the case a = y. The single-qubit rotation gates acting on the initial state $|\mathbf{0}\rangle$ generate superpositions supported on the set of Pauli strings

$$\{\mathbb{I},\sigma^x,\sigma^z\}^{\otimes n}.$$

It is therefore crucial to determine how this set transforms under the entangling layer composed of nearest-neighbor controlled-Z gates,

$$\left(\prod_{i=1}^{n-1} CZ_{i,i+1}\right) \{\mathbb{I}, \sigma^x, \sigma^z\}^{\otimes n} \left(\prod_{i=1}^{n-1} CZ_{i,i+1}\right).$$

For each pair of neighboring qubits (i, i + 1), the controlled-Z gate acts on local Pauli operators according to the

following transformation rules:

P	$CZ_{i,i+1} P CZ_{i,i+1}$
	$\begin{array}{c} \mathbb{I} \otimes \mathbb{I} \\ \mathbb{I} \otimes \sigma^x_{i+1} \\ \sigma^z_i \sigma^y_{i+1} \\ \mathbb{I} \otimes \sigma^z_{i+1} \end{array}$
$\begin{array}{c} \sigma_i^x \otimes \mathbb{I} \\ \sigma_i^x \sigma_{i+1}^x \\ \sigma_i^x \sigma_{i+1}^y \\ \sigma_i^x \sigma_{i+1}^z \end{array}$	$\sigma_i^x \otimes \mathbb{I} \ \sigma_i^x \sigma_{i+1}^x \ \sigma_i^y \sigma_{i+1}^x \ \sigma_i^x \sigma_{i+1}^z$
$\begin{array}{l} \sigma_i^y \otimes \mathbb{I} \\ \sigma_i^y \sigma_{i+1}^x \\ \sigma_i^y \sigma_{i+1}^y \\ \sigma_i^y \sigma_{i+1}^z \end{array}$	$\begin{matrix}\sigma_i^y\sigma_{i+1}^z\\\sigma_i^x\sigma_{i+1}^y\\-\sigma_i^y\sigma_{i+1}^y\\\sigma_i^y\sigma_{i+1}^z\\\sigma_i^y\sigma_{i+1}^z\end{matrix}$
$egin{array}{l} \sigma_i^z \otimes \mathbb{I} \ \sigma_i^z \sigma_{i+1}^x \ \sigma_i^z \sigma_{i+1}^y \ \sigma_i^z \sigma_{i+1}^z \end{array}$	$\sigma_i^z \otimes \mathbb{I} \ \sigma_i^z \sigma_{i+1}^x \ \sigma_i^z \sigma_{i+1}^y \ \sigma_i^z \sigma_{i+1}^y \ \sigma_i^z \sigma_{i+1}^z$

From this table, we observe that a σ_y operator appears on a given qubit whenever a σ_x operator in the input string is adjacent to another σ_x on a neighboring qubit.

Therefore, determining whether a Pauli string produces at least one σ_y under the full chain of CZ gates is equivalent to checking whether the original string contains two consecutive σ_x operators. The problem is thus reduced to a purely combinatorial one: counting the number of length-n strings over the alphabet $\{\mathbb{I}, \sigma^x, \sigma^z\}$ that contain at least one pair of adjacent σ_x symbols.

Denoting by a_n the number of strings without adjacent σ_x symbols, the number of strings that generate at least one σ_y is

$$N_{\nu}(n) = 3^n - a_n.$$

The quantity a_n satisfies the recurrence relation

$$a_n = 2a_{n-1} + 2a_{n-2}, \qquad a_1 = 3, \quad a_2 = 8,$$

where the first term counts strings beginning with \mathbb{I} or σ_z , and the second term counts strings starting with σ_x followed by a non- σ_x symbol.

Finally, since adding further layers does not increase the number of strings associated with the λ_M minimum, we conclude that the number of right eigenvectors contributing to the evaluation of the noise resilience is precisely N_y .

Using analogous arguments, in the complementary case a = x, the number of eigenvectors associated with the minimum is $\tilde{N}_y = a_n$. For the case studied numerically, n = 8, we find

$$N_y = 3217, \qquad \tilde{N}_y = 3344,$$

which implies that the ansatz with a = y is more noise-resilient as observed.